


Article

# Dual pH- and GSH-Responsive Degradable PEGylated Graphene Quantum Dot-Based Nanoparticles for Enhanced HER2-Positive Breast Cancer Therapy

Na Re Ko <sup>1,2,†</sup> , Se Young Van <sup>1,2,†</sup>, Sung Hwa Hong <sup>3</sup>, Seog-Young Kim <sup>4</sup>, Miran Kim <sup>2</sup>, Jae Seo Lee <sup>5</sup>, Sang Ju Lee <sup>2</sup>, Yong-kyu Lee <sup>6</sup>, Il Keun Kwon <sup>5</sup> and Seung Jun Oh <sup>2,\*</sup>

<sup>1</sup> Biomedical Research Center, Asan Institute for Life Sciences, 88 Olympic-ro 43-gil, Songpa-gu, Seoul 05505, Korea; nare.ko@amc.seoul.kr (N.R.K.); sey.van88@gmail.com (S.Y.V.)

<sup>2</sup> Department of Nuclear Medicine, Asan Medical Center, University of Ulsan College of Medicine, 88 Olympic-ro 43-gil, Songpa-gu, Seoul 05505, Korea; ranaranmi@naver.com (M.K.); atlas425@amc.seoul.kr (S.J.L.)

<sup>3</sup> Department of Chemical Engineering and Applied Chemistry, University of Toronto, 200 College Street, Toronto, ON M5S 3E5, Canada; sunghwa.hong@mail.utoronto.ca

<sup>4</sup> Department of Convergence Medicine, University of Ulsan College of Medicine, 88 Olympic-ro 43-gil, Songpa-gu, Seoul 05505, Korea; ksy0222@gmail.com

<sup>5</sup> Department of Dental Materials, School of Dentistry, Kyung Hee University, 26 Kyungheedaero, Dongdaemun-gu, Seoul 02447, Korea; leejs8433214@naver.com (J.S.L.); kwoni@khu.ac.kr (I.K.K.)

<sup>6</sup> Department of Chemical & Biological Engineering, Korea National University of Transportation, 50 Daehak-ro, Chungcheongbuk-do, Cheongju 27469, Korea; leeyk@ut.ac.kr

\* Correspondence: sjoh@amc.seoul.kr; Tel.: +82-2-3010-4595

† These authors contributed equally to this work.

Received: 28 November 2019; Accepted: 29 December 2019; Published: 2 January 2020



**Abstract:** Dual stimuli-responsive degradable carbon-based nanoparticles (DS-CNPs) conjugated with Herceptin (HER) and polyethylene glycol (PEG) have been designed for the treatment of HER2-positive breast cancer. Each component has been linked through disulfide linkages that are sensitive to glutathione in a cancer microenvironment.  $\beta$ -cyclodextrin ( $\beta$ -CD) on the surface of DS-CNPs formed an inclusion complex (DL-CNPs) with doxorubicin (DOX) at a high loading capacity of  $5.3 \pm 0.4\%$ . In response to a high level of glutathione (GSH) and low pH in a tumor environment, DL-CNPs were rapidly degraded and released DOX in a controlled manner via disruption of host–guest inclusion. These novel DL-CNPs exhibited high cellular uptake with low toxicity, which induced the efficient inhibition of antitumor activity both in vitro and in vivo. Cell viability, confocal laser scanning microscopy, and animal studies indicate that DL-CNPs are a great platform with a synergistically enhanced antitumor effect from the dual delivery of HER and DOX in DL-CNPs.

**Keywords:** stimuli-responsive degradation system; glutathione; breast cancer; Herceptin; active targeting; PEGylation

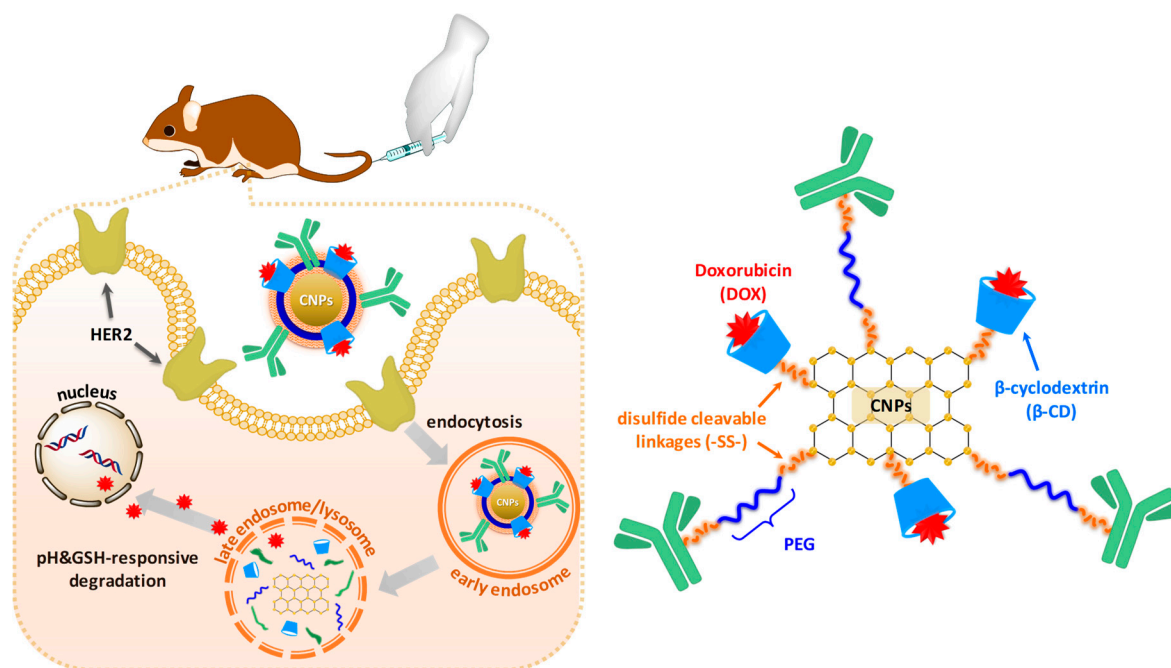
## 1. Introduction

Recently, stimuli-responsive degradation (SRD)-induced drug delivery systems (DDS) have received much attention in the field of nanomedicine. SRD enables nanotechnology-based DDS to achieve both selective uptake at target disease sites and controlled drug release with low side effects. SRD-nanomedicine platforms can be engineered with dynamic covalent linkages that can be cleaved in response to external stimulus such as glutathione (L- $\gamma$ -glutamyl-L-cysteinyl-glycine;

GSH), pH, enzymes, temperature, and glucose. These environmental triggers are considered safe and efficient as stimuli-responsive nanocarriers for cancerous diseases [1–3]. In particular, GSH is an antioxidant that maintains the intracellular redox balance, and elevated GSH levels are associated with chemoresistance of neoplastic tissue [4–6]. GSH is distributed at different concentrations within the tumor milieu such as in the intracellular compartments of a tumor cell at 2–10 mM, and in the extracellular compartments of a tumor cell at <20  $\mu$ M [7,8]. Disulfide linkages are cleavable by a reductive environment or a disulfide-thiol exchange reaction [9–11], and upon exposure to GSH, cleavage of the disulfides accelerates destabilization of disulfide-labeled drug carriers and controls the release of encapsulated anticancer therapeutics within the carriers [12]. In addition, the pH difference between tumor/inflamed regions (pH 5.4–7.1) and normal tissue/blood stream (pH ~7.4) enables cancer cells to promote cell–matrix remodeling, increase the activity of acid-activated proteases, and progress tumor growth [13,14]. Such a difference in the tumor microenvironment is useful tools for designing cancer-specific multifunctional biomimetic nanoparticles. Various pH-responsive degradable drug carriers possess acid-labile cleavable linkages such as ester [15,16], amide [17,18], and ketal/acetal groups [19,20].

Carbon-based nanoparticles (CNPs) including graphenes, carbon nanotubes, and fullerenes, have become attractive materials in the field of biomedical applications [21]. Due to their good biocompatibility, and structural, physical, and chemical properties, CNPs have been investigated for their use as biosensors, drug delivery carriers, and in imaging probes [22]. Surface-functionalized CNPs enable modifications and conjugations with chemical/biomolecular agents such as drugs, antibodies, and immunoglobulin [23–25]. In this respect, a Herceptin (HER)-conjugated GSH-responsive degradable graphene quantum dot (GQD)-based nanomaterial has been developed to target HER2-positive breast cancer [26]. HER2 (Human Epidermal growth factor Receptor 2) is a protein on the surface of breast cells made by HER2 genes. Overexpressed HER2 genes produce up to 100-fold of HER2 proteins and also cause uncontrolled cell growth, which leads to HER2-positive breast cancer [27]. HER is a FDA-approved monoclonal antibody that binds to HER2 to inhibit intracellular signaling and induce the immune response of HER2-overexpressed breast cancer [28,29]. However, due to the low antitumor efficiency of HER, chemotherapy is required to enhance anticancer activity for clinical use [30]. Polyethylene glycol (PEG)-labeled GQDs enable a prolonged blood circulation time and have a stealth effect on the host immune system. In addition, disulfides at conjugate junctions have been cleaved in response to the high GSH level in breast cancer cells and enable the controlled release of biomolecular- (HER) and chemo-anticancer therapeutics (doxorubicin; DOX). However, such multiple stimuli-responsive graphenes have seldom been reported [31] and dual redox- and pH-responsive GQD-based nanocarriers for breast cancer therapy have not been investigated to date.

In this study, novel dual stimuli-responsive graphene quantum dot-based multi-functional carbon nanoparticles (DS-CNPs) were developed for use in breast cancer therapy (Scheme 1). The particles were modified with both PEG and HER, and they have pH-dependent ester/amide bonds and GSH-sensitive disulfide linkages at multiple locations. A drug pocket  $\beta$ -cyclodextrin ( $\beta$ CD) with a hydrophobic cavity and hydrophilic surface enhances the solubility of the hydrophobic anticancer drug, DOX, via host–guest chemistry. In addition,  $\beta$ CD is known to release possessing drugs in response to multiple external stimuli including temperature, changes in pH or redox, light, and competitive binding [32–34]. These engineered drug carriers allow not only active targeting, but they also enhance the anticancer effect with the controlled release of HER therapeutics. When DOX-loaded DS-CNPs (DL-CNPs) larger than 200 nm are intravenously injected, they accumulate in the breast cancer region via an enhanced permeability and retention effect. After endocytosis of DL-CNPs, both HER and DOX are released upon exposure to low pH and a high level of GSH. HER not only specifically guides the DL-CNPs to HER2-positive breast cancer, but it also suppresses tumor growth [35]. The released DOX then penetrates the cell nucleus and causes cell death by damaging the DNA [36]. Combined, the cell viability, confocal laser scanning microscopy (CLSM), and in vivo studies suggest that DL-CNPs have great potential for use in the treatment of HER2-positive breast cancer.



**Scheme 1.** Illustration of cellular uptake and drug release of DOX-loaded DS-CNPs (DL-CNPs) in HER2-positive breast cancer cells.

## 2. Materials and Methods

### 2.1. Materials

Amine-functionalized CNPs were synthesized by the pyrolysis of L-glutamic acid (the detailed procedure is described in our previous report [25]). 3,3'-Dithiodipropionic acid (SS-COOH, 99%), polyethylene glycol (PEG, MW = 3000 g/mol), 1-ethyl-3-(3-dimethylaminopropyl)-carbodiimide (EDC, >97%), 4-dimethylaminopyridine (DMAP, >98%), N-hydroxysuccinimide (NHS, 98%), and doxorubicin hydrochloride (DOX,  $-\text{NH}_3^+\text{Cl}^-$  salt form, >98%) were obtained from Aldrich (St. Louis, MO, USA), and  $\beta$ CD (>98%) obtained from TCI (Tokyo, Japan) were purchased and used as received. HER was purchased from Roche (Basel, Switzerland), and Roswell Park Memorial Institute (RPMI) 1640 media, Dulbecco's phosphate-buffered saline, trypsin-EDTA, and penicillin-streptomycin were purchased from Thermo Fisher Scientific (Waltham, MA, USA). Fetal bovine serum (FBS), CCK-8 reagent (product # CK04-13), and lysosomal staining reagent (product # ab176829) were purchased from GIBCO BRL (Grand Island, NY, USA), Dojindo (Kumamoto, Japan), and Abcam (Cambridge, MA, USA), respectively.

### 2.2. Instrumentation

The synthesis of  $\beta$ CD-SS-COOH, PEG-(SS-COOH)<sub>2</sub> was confirmed by Fourier transform nuclear magnetic resonance spectrometer (NMR, AVANCE III HD400, Bruker, Rheinstetten, Germany); and  $\beta$ CD-SS-CNPs and DS-CNPs were characterized by Fourier transform infrared (FTIR) spectroscopy (Thermo Scientific Nicolet 380 spectrometer, Waltham, MA, USA) using the KBr Pellet technique with scanning in the wavenumber range 400–4000  $\text{cm}^{-1}$ . The conjugation of HER with PEG-(SS-COOH)<sub>2</sub> was confirmed by x-ray photoelectron spectroscopy (XPS, Thermo Fisher, K-alpha, East Grinstead, UK). UV/Vis spectra were recorded using a PerkinElmer Lambda 650S UV/Vis spectrometer (Waltham, MA, USA). Thermal gravimetric analysis (TGA) was conducted to confirm the synthesis of DS-CNPs using TA Instruments 2960 SDT V3.0F (New Castle, DE, USA, 10 °C/min, 10–800 °C, at atmospheric pressure under nitrogen flow). The change in particle size during synthesis was evaluated by dynamic light scattering (DLS) using a particle size analyzer (ELSZ-1000, Otsuka Electronics Co. Ltd., Osaka, Japan).

### 2.3. Carboxylation of $\beta$ CD and Conjugation with CNPs ( $\beta$ CD-SS-CNPs)

In a solution of SS-COOH (5.56 g, 26.4 mmol) dissolved in 20 mL DMF, DMAP (108 mg, 0.88 mmol) was added and stirred at 50 °C for 10 min.  $\beta$ CD (10 g, 8.8 mmol) was dissolved in 10 mL DMF and added to a mixture of SS-COOH/DMAP. Finally, EDC (1.37 g, 8.8 mmol) dissolved in 10 mL DMF was added, and the reaction mixture was stirred at 50 °C for 24 h. The resulting  $\beta$ CD-SS-COOH was obtained by dialysis (MWCO = 1000 g/mol) against distilled water (DW) for two days and lyophilization. The purified and dried  $\beta$ CD-SS-COOH (500 mg) was dissolved in the presence of DMAP (27 mg, 0.22 mmol) in 30 mL PBS and added drop-wise into a solution of 35 mg CNPs and EDC (64 mg, 0.41 mmol) in PBS (5 mL). The reaction mixture was stirred in the dark at room temperature (RT) for two days. The solution was filtered, and the filtrates were dialyzed using dialysis tubing (MWCO = 1000 g/mol) against DW for two days to remove residual by-products and then lyophilized.

### 2.4. Carboxylation of PEG and Conjugation with HER (SS-PEG-SS-HER)

SS-PEG-SS-HER was synthesized by the click reaction (the detailed procedure is described in our previous report) [26]. In brief, two hydroxyl end groups of PEG were substituted by SS-COOH, which resulted in PEG-(SS-COOH)<sub>2</sub>. SS-PEG-SS-HER was then synthesized by an EDC coupling reaction between PEG-(SS-COOH)<sub>2</sub> and HER in the presence of DMAP. The purified SS-PEG-SS-HER was then lyophilized and stored at 4 °C until further use.

### 2.5. Synthesis of Dual Stimuli-Responsive Degradable CNPs (DS-CNPs)

SS-PEG-SS-HER (500 mg, 0.0034 mmol) was dissolved in 30 mL PBS in the presence of DMAP (212 mg, 1.7 mmol). EDC (2.7 g, 17.8 mmol) and NHS (2.0 g, 17.4 mmol) were then added and stirred for 10 min, and  $\beta$ CD-SS-CNPs was added in a solution and stirred at room temperature (RT) for 24 h. The resulting mixture was filtered, and the filtrates were then dialyzed using dialysis tubing (MWCO = 1000 g/mol) against DW for two days. DS-CNPs were lyophilized and stored at 4 °C until further use.

### 2.6. Preparation DOX-Loaded DS-CNPs (DL-CNPs)

DS-CNPs (20 mg) were dissolved in 2 mL DMSO in the presence of 2 mg DOX and Et<sub>3</sub>N (3 molar equivalents to DOX) and stirred at RT for 24 h. PBS (58 mL) was then added drop-wise into the solution and stirred at RT for 24 h. The mixture was transferred into a dialysis membrane (MWCO = 1000 g/mol) and dialyzed against 1 L DW for 24 h and PBS buffered for 24 h. To determine the loading capacity (LC) and encapsulation efficiency (EE) of DOX in DL-CNPs, an aliquot of the DL-CNPs was mixed with DMF (1:3 v/v). Then, the amount of encapsulated DOX was measured using the Beer–Lambert equation with the absorbance at  $\lambda_{\text{max}} = 498$  nm and the previously reported extinction coefficient ( $\epsilon = 12,800 \text{ M}^{-1} \text{ cm}^{-1}$ ) [25]. The LC and EE of DL-CNPs were calculated as follows;

$$\text{LC} = \frac{\text{weight of DOX in DL - NPs}}{\text{total weight of DL - NPs}}$$

$$\text{EE} = \frac{\text{weight of DOX in DL - NPs}}{\text{initial amount of DOX added}}$$

### 2.7. pH and GSH-Triggered Release of DOX from DL-CNPs

DL-GQD solution (3 mL) was placed in dialysis tubing (MWCO = 1000 g/mol) and then dialyzed against 50 mL PBS buffer under different conditions: 10 mM GSH at pH 5.5; 10 mM GSH at pH 7.4; 2  $\mu$ M GSH at pH 5.5; and 2  $\mu$ M GSH at pH 7.4 as the control. All experiments were conducted in the dark to prevent DOX from decomposing. The absorbance of DOX in outer water was taken periodically for 48 h using a UV/Vis spectrometer at  $\lambda_{\text{ex}} = 498$  nm.

## 2.8. Cell Culture

Both cell types were cultured in RPMI 1640 containing L-glutamine, 25 mM HEPES, 10% fetal bovine serum, and 1% antibiotics (50 units/mL penicillin and 50 units/mL streptomycin). Cells were incubated at 37 °C in a humidified atmosphere containing 5% CO<sub>2</sub> until appropriate confluency, and fresh media were provided every 3–4 days.

## 2.9. Protein Preparation and Immunoblot Analysis

SK-BR-3 and MDA-MB-231 cells were harvested with 1X PBS buffer and suspended in lysis buffer (Cell Signaling Technology, Beverly, MA, USA), then boiled for 5 min. Protein concentrations were measured with the BCA protein assay (Pierce, Rockford, IL, USA). The samples were diluted with 1X lysis buffer and an equal amount of protein was loaded on 10% SDS-polyacrylamide gel. SDS-polyacrylamide gel electrophoresis (PAGE) analysis was performed using a Bio-rad gel apparatus. Proteins were separated by SDS-PAGE, transferred to nitrocellulose membranes, and blocked with 5% skim milk in TBS-Tween 20 (0.05%) for 30 min. The membrane was incubated with primary antibodies against HER/ErbB2 (Cell Signaling Technology, Danvers, MA, USA) and  $\beta$ -actin (Sigma, St. Louis, MO, USA) overnight at 4 °C. Horseradish peroxidase-conjugated anti rabbit IgG used as the secondary antibody (Jackson immunoresearch, West Grove, PA, USA) was incubated with the membrane for 1 h at RT. Protein quantification analysis was performed using the CS Analyzer 4 program (ATTO corporation, Tokyo, Japan).

## 2.10. Cell Viability Using the CCK-8 Assay

SK-BR-3 and MDA-MB-231 cells were seeded at a density of  $5 \times 10^3$  cells per well into a 96-well plate ( $n = 3$ ) in 100  $\mu$ L of RPMI 1640 media, and were then allowed to adhere on the substrate for 3 h. Cells were then treated with DS-CNPs (0–500  $\mu$ g/mL), DL-CNPs (0–40  $\mu$ g/mL), and equivalent amounts of free DOX (calculated from the LC) at the same concentration ranges of 0 to 3.67  $\mu$ M for 48 h. The culture media were then aspirated, and 100  $\mu$ L of fresh media with 10  $\mu$ L of CCK-8 reagent was added in every well and then incubated for 2 h at 37 °C. The absorbance value was measured at 450 nm using a microplate spectrophotometer (Infinite 200 Pro, Tecan, Switzerland).

## 2.11. Confocal Laser Scanning Microscopy (CLSM)

SK-BR-3 and MDA-MB-231 cells were plated on a glass bottom cell culture confocal dish ( $\Phi$  20 mm) at a density of  $1 \times 10^5$  cells per well and then incubated for 24 h under 37 °C and 5% CO<sub>2</sub> in a humidified incubator. At 24 h, cells were treated with both DL-CNPs (43.48  $\mu$ g/mL) and free DOX (4.0  $\mu$ M, which is an equivalent amount to the DL-CNPs) in a time-dependent manner (3 h and 8 h). Lysosomal staining reagent diluted, according to the manufacturer's protocols, was incubated with cells for 30 min before observation to clarify the cytoplasm area. DOX and lysosomal staining reagent were observed at a wavelength of excitation/emission of 488/589 nm and 633/665 nm, respectively, using a confocal laser scanning microscope (LSM 880, ZEISS, Oberkochen, Germany).

Fluorescence images were quantified using ImageJ software (NIH). A total of 30 cells were randomly selected from each experimental group for image analysis (an average of 10 cells per image). The DOX uptake within the nucleus was analyzed based on the fluorescence intensity ratio of the nucleus to the whole cell area. The mean gray value of the nucleus divided by that of the whole cell area was presented as a percentage. A statistical analysis of the data was conducted using GraphPad Prism 5 (GraphPad Software, San Diego, CA, USA). The student *t*-test was applied to compare two time points of the DL-CNP groups in each cell, and the statistical significance was denoted as \* ( $p < 0.05$ ), \*\* ( $p < 0.01$ ), or \*\*\* ( $p < 0.001$ ).

## 2.12. Animal Studies

The research protocol was approved by the Institutional Animal Care and Use Committee of the Asan Institute for Life Science (registration no. 2018-13-066). Athymic nude mice (Balb/c-nu, female,

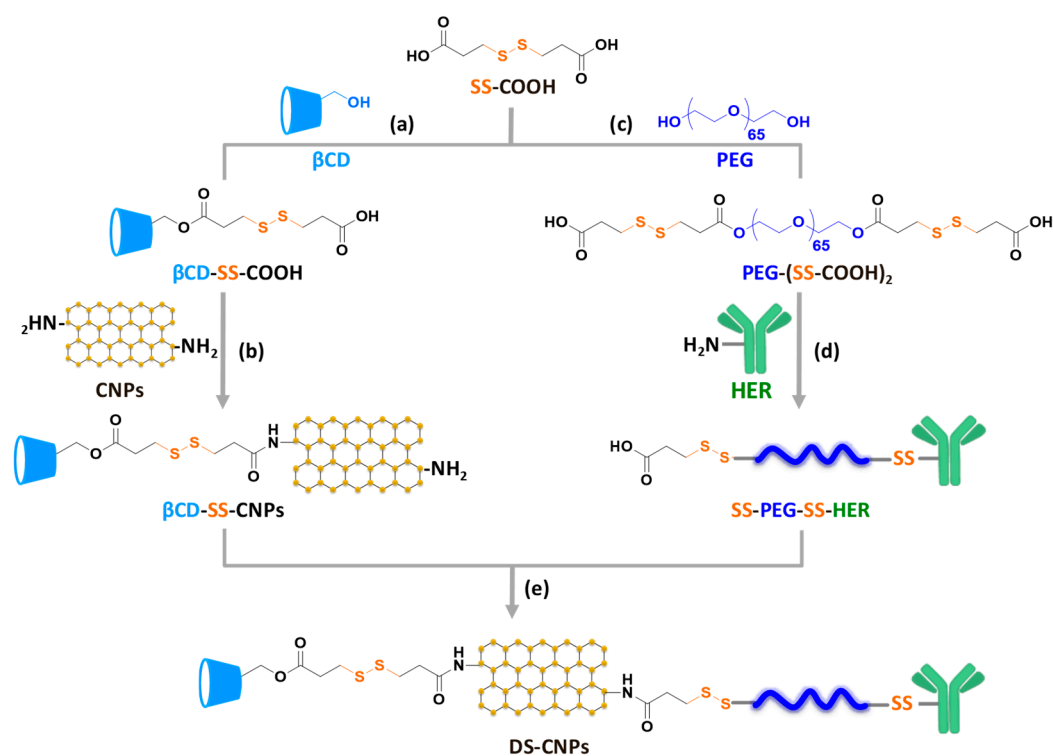


5–6 weeks old, 20–22 g) and NSG mice (female, 5–6 weeks old, 20 g) were purchased from the Japan Shizuoka Laboratory Center. Mice were maintained in accordance with the Institutional Animal Care and Use Committee guidelines of the Asan Institute for Life Science. Mice were inoculated with exponentially growing human breast cancer cells (MDA-MB-231 or SK-BR-3, 1:1 ratio of plain media and Matrigel (Corning, 354234,  $1 \times 10^7$ /total 0.2 mL) into the flank subcutaneously. Over the following 14 to 25 days, tumors were allowed to reach a volume of 70 to 100 mm<sup>3</sup>, and the tumor volume was calculated by the length  $\times$  width  $\times$  height  $\times \pi/6$ . Mice were randomly allocated to the PBS, free DOX, or DL-CNPs treatment group ( $n \geq 7$  per group), and injected intravenously with vehicles or drugs bearing the xenograft once a week until the end point on day 27 to 38. Immunohistochemical analysis was also carried out with sectioned samples using Ki-67 (cat. No. M7240, Agilent Dako).

### 3. Results and Discussions

#### 3.1. Synthesis and Characterization of DS-CNPs

Scheme 2 illustrates the synthetic approach used to prepare dual stimuli-responsive degradable DS-CNPs consisting of  $\beta$ -CD and HER with multiple disulfide linkages.



**Scheme 2.** Synthetic scheme of dual stimuli-responsive degradable carbon-based nanoparticles (DS-CNPs): carboxylation of  $\beta$ -cyclodextrin ( $\beta$ -CD) (a), conjugation of carbon-based nanoparticles (CNPs) (b), carboxylation of polyethylene glycol (PEG) (c), conjugation of Herceptin (HER) (d), and coupling reaction used to form DS-CNPs (e) via EDC/DMAP coupling reaction.

SS-COOH was labeled with  $\beta$ -CD and PEG separately via a facile DCC/DMAP coupling reaction to produce  $\beta$ -CD-SS-COOH and PEG-(SS-COOH)<sub>2</sub>. Synthesis of  $\beta$ -CD-SS-COOH and PEG-(SS-COOH)<sub>2</sub> was clearly determined by <sup>1</sup>H-NMR (Figure 1a,c). Carboxylic acid groups of  $\beta$ -CD-SS-COOH were then covalently attached on the amine-functionalized CNPs to introduce pH-responsive amide bonds between  $\beta$ -CD and CNPs, and the formation of amide groups was confirmed by FTIR (Figure 1b). A carboxylic acid group of PEG-(SS-COOH)<sub>2</sub> was utilized to conjugate with the amine groups on HER. The increase in N content determined by XPS indicated the formation of SS-PEG-SS-HER (Figure 1d). Amine groups on the surface of partially modified  $\beta$ -CD-SS-CNPs were then used to

synthesize DS-CNPs via a coupling reaction with the remaining carboxylic acid of SS-PEG-SS-HER. The successful synthesis of DS-CNPs was determined by both the changes in the chemical bonds and the thermal properties. In Figure 1e, the appearance of a new peak at  $1545\text{ cm}^{-1}$  showed the presence of amide bonds between  $\beta$ CD-SS-CNPs and SS-PEG-SS-HER. TGA analysis showed a single transition in weight loss at  $195\text{ }^\circ\text{C}$  for  $\beta$ CD-SS-CNPs and two temperature transitions at  $180\text{ }^\circ\text{C}$  and  $270\text{ }^\circ\text{C}$  for SS-PEG-SS-HER. After conjugation, DS-CNPs underwent three temperature transitions at  $210\text{ }^\circ\text{C}$ ,  $280\text{ }^\circ\text{C}$ , and  $340\text{ }^\circ\text{C}$ , which indicates that the DS-CNPs possessed both  $\beta$ CD-SS-CNPs and SS-PEG-SS-HER components. After surface modification, the particle sizes of DS-CNPs significantly increased from  $28.8 \pm 6.7\text{ nm}$  to  $245.0 \pm 10.0\text{ nm}$  (Figure 2a).

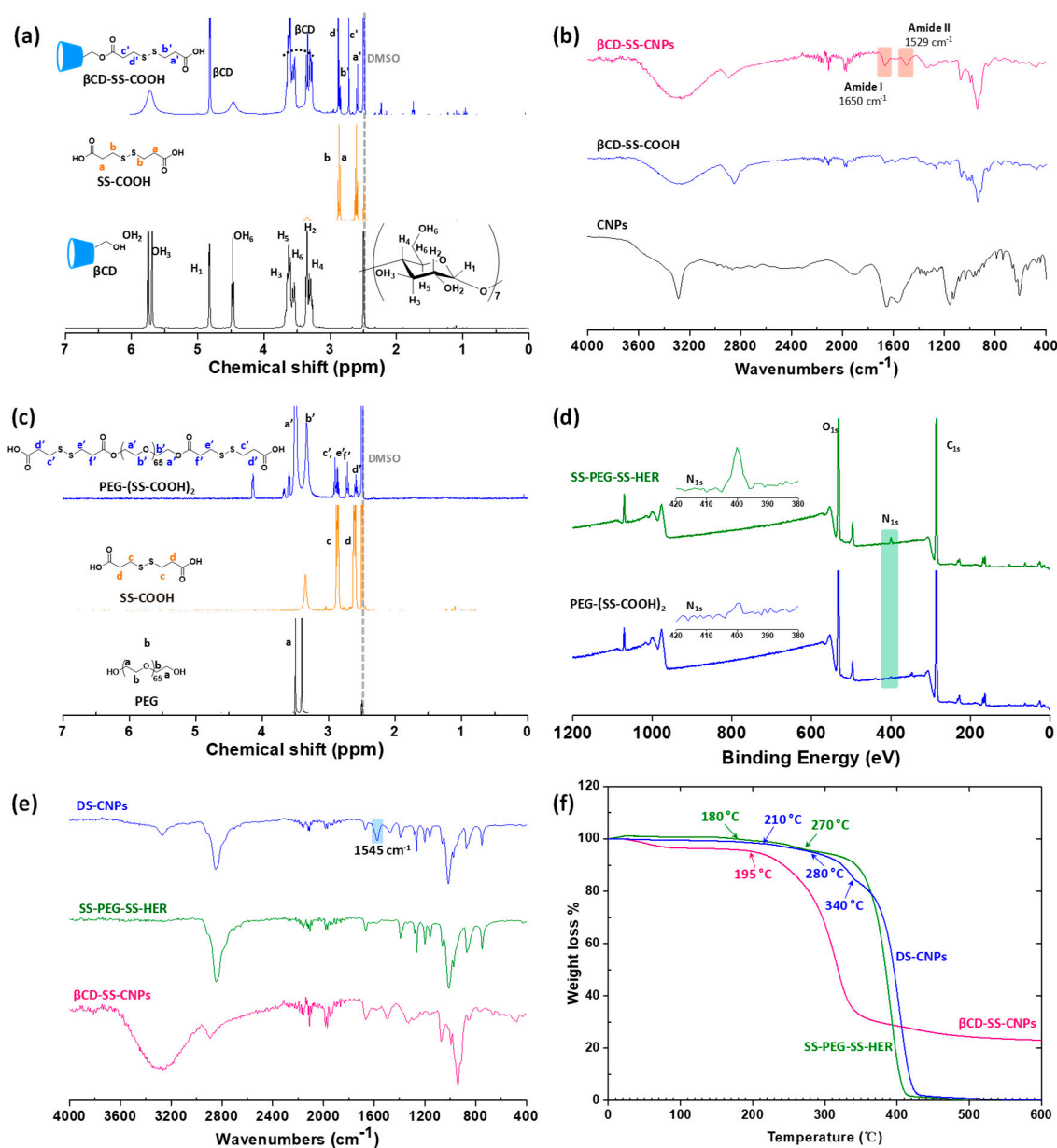


**Figure 1.** (a) Synthesis of  $\beta$ CD-SS-COOH confirmed by  $^1\text{H-NMR}$ , (b) synthesis of  $\beta$ CD-SS-CNPs confirmed by FTIR, (c) synthesis of PEG-(SS-COOH) $_2$  confirmed by  $^1\text{H-NMR}$ , (d) synthesis of SS-PEG-SS-HER confirmed by XPS, synthesis of DS-CNPs confirmed by FTIR (e) and TGA (f).

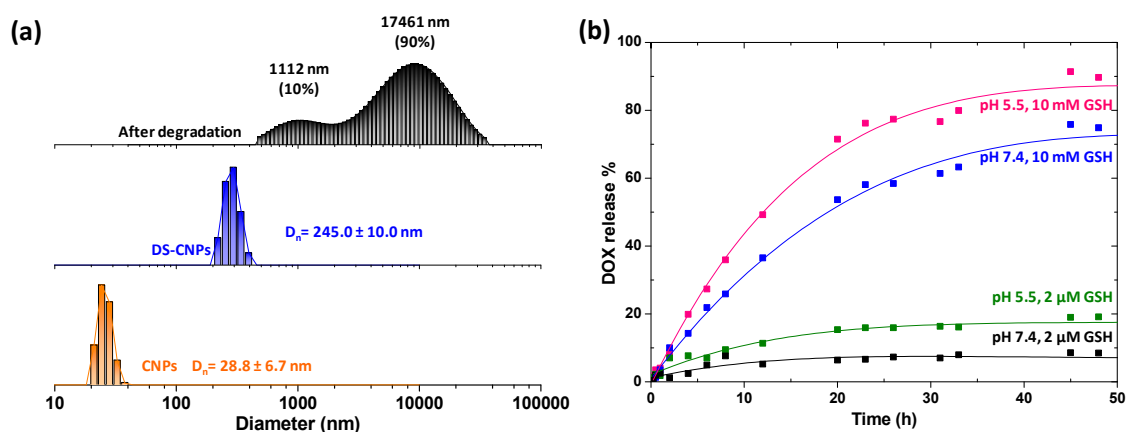


**Figure 2.** (a) DLS diagrams of CNP, DS-CNPs, and degraded DL-CNPs, (b) in vitro release profile of DOX from DL-CNPs under various conditions: 10 mM GSH at pH 5.5, 10 mM GSH at pH 7.4, 2  $\mu$ M GSH at pH 5.5, and 2  $\mu$ M GSH at pH 7.4 as the control.

### 3.2. Loading and External Stimuli-Trigger Release of DOX

DOX is an anticancer drug with poor water solubility. In the design of DS-CNPs,  $\beta$ CD can load DOX into the hydrophobic cavity via host–guest chemistry during dialysis. The LC and EE of DL-CNPs were determined as  $5.3 \pm 0.4\%$  and  $26.5 \pm 1.8\%$ , respectively. These values were comparable to the  $\beta$ CD-labeled CNP models described in our previous study [25].

The DOX release profile of the DL-CNPs was investigated under different conditions mimicking the tumor microenvironment for 48 h. At 37 °C, DL-CNPs were exposed to different GSH concentrations (10 mM and 2  $\mu$ M) at different pH (5.5 and 7.4). As shown in Figure 2b, >90% of DOX was rapidly released from the DL-CNPs at pH 5.5 in the presence of the 10 mM GSH concentration, which is a similar environment to that of breast cancer. Interestingly, ~80% of DOX was released under pH 7.4 in the presence of 10 mM GSH, which was significantly higher than that with 2  $\mu$ M GSH at pH 5.5 (<20%). Indeed, the effect of GSH was greater than that of pH on the release of DOX from DL-CNPs.

Typically,  $\beta$ CDs are directly conjugated on the surface of nanoparticles and the drug is loaded in  $\beta$ CD. The drugs are partly exposed to the outer environment so external triggers can easily interfere with the drug– $\beta$ CD interaction, causing drug release. This conventional  $\beta$ CD-based drug delivery platform exhibited a significantly slow drug release rate at low pH [37–40]. However, the drug release of DL-CNPs was not the same as other  $\beta$ CD-possessing nanoparticles due to its unique structure. To explain the release kinetics of DL-CNPs, two main factors were considered: steric hindrance and host–guest chemistry. In this research, the surface of the DL-CNPs was modified with two different blocks: a block consisting of SS- $\beta$ CD branches for drug loading and another block consisting of SS-PEG-SS-HER for PEGylation. Compared to the SS- $\beta$ CD branches, PEGylated HER branches (SS-PEG-SS-HER) were long, bulky, hydrophilic, and flexible. In an aqueous environment, SS-PEG-SS-HER chains surround the small SS- $\beta$ CD blocks on the surface of CNPs to improve the solubility of DL-CNPs and the protection of DOX in  $\beta$ CD from premature release in blood vessels [41–43]. When the DL-CNPs are delivered to the tumor, they are degraded in response to the high concentration of GSH, and DOX in  $\beta$ CD is released with exposure to an acidic environment. In order to release more DOX from DL-CNPs, steric-hindered SS-PEG-SS-HER chains should be degraded to dissociate PEGylation layer and host–guest chemistry is disrupted by external stimuli. Due to the unique characteristics of a GSH-responsive degradation system with disulfides, our platform exhibited slow and low drug release kinetics of DL-CNPs in the presence of 2  $\mu$ M GSH at pH 5.5, compared to 10 mM GSH at pH 7.4.

The size of the degraded DL-CNPs was characterized using DLS (Figure 2a). DS-CNPs were found to have a stable and monomodal distribution with an average diameter of ~245 nm, whereas large aggregates formed after the degradation of DL-CNPs. This result supports the destabilization of DL-CNPs after cleavage of disulfide linkages and the release of DOX in a rapid and controlled manner.



### 3.3. Evaluation of Active Targeting and Intracellular Accumulation In Vitro

The selective targeting properties of anticancer drug carriers are key in enhancing their anticancer efficacies and reducing side effects. The significant difference in HER2 levels between HER2-negative and HER2-positive breast cancer enables HER-containing drug carriers to access HER2-positive breast cancer [44–46]. Prior to in vitro studies, validation of HER2 expression in the SK-BR-3 and MDA-MB-231 cell lines was conducted with SDS-PAGE and immunoblot analysis. Membranes were incubated with antibodies against HER2 and  $\beta$ -actin for standardization to control the loading variability. As shown in Figure S1, SK-BR-3 expresses a greater amount of HER2 compared to MDA-MB-231 and these results suggest that the difference in cell viability could be attributed to the abundance of HER2 receptors that changes the fate of nanoparticles [47].

The in vitro cellular uptake of DS-CNPs in SK-BR-3 (HER2-positive) and MDA-MB-231 (HER2-negative) was evaluated by comparing cell viability after incubation for 48 h. As shown in Figure 3a the viability of SK-BR-3 cells gradually decreased with an increase in the amount of DS-CNPs, whereas the viability of the MDA-MB-231 cells was >96% at up to 500  $\mu\text{g}/\text{mL}$ , which suggests that DS-CNPs have low toxicity to HER2-negative cells. These results indicate that DS-NPs have an excellent active targeting ability toward HER2-positive breast cancer, but a high dose of DS-NPs is required to achieve the desired cytotoxicity. Many clinical trials have reported that treatment of HER alone has a low response rate against the extracellular domain of HER-2-positive breast cancer [48–51]. On the other hand, a combination therapy with chemotherapeutic drugs promotes not only the inhibition of tumor growth, but also the overall survival rate of breast cancer patients [52–56]. To determine the synergistic effect of combination therapy with HER and DOX, the viability of DL-CNPs in SK-BR-3 cells was compared with that in MDA-MB-231 cells. Figure 3b shows significantly decreased cell viability values of SK-BR-3 compared with the viability of MDA-MB-231 incubated at the same DL-CNPs concentration.

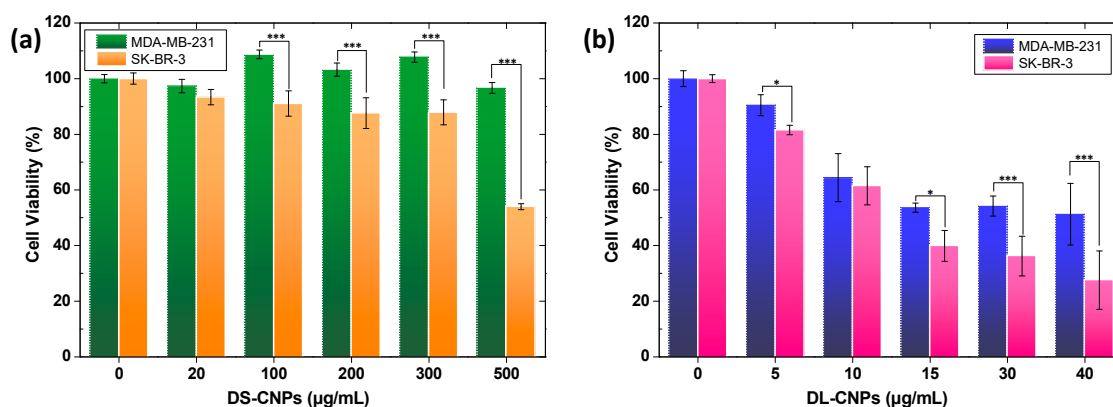


**Figure 3.** Cytotoxicity of (a) DS-CNPs and (b) DL-CNPs in SK-BR-3 and MDA-MB-231 cells after 48 h incubation ( $n = 6$ , \*  $p < 0.05$ , \*\*\*  $p < 0.001$ ).

To determine the uptake specificity and sequential release of DOX, the DL-NPs and free DOX were incubated in SK-BR-3 and MDA-MB-231 cells, respectively, and the intracellular uptake and localization were investigated by CLSM at different time points (3 h and 8 h). As seen in Figure 4, the red DOX fluorescence intensity percentage was quantified by the ratio of the nucleus to the whole cell area. For comparison, the amount of free DOX was adjusted to be equivalent to the amount of DOX encapsulated in DL-CNPs. Strong intensity in the CLSM images was expected since DOX internalizes into the cells via passive diffusion. After 3 h of incubation, a strong red-color signal corresponding to DOX entrapped in DL-CNPs was widely distributed in the cytoplasm of SK-BR-3, whereas a weak red fluorescence was evident in MDA-MB-231. Similar fluorescence intensity of the DOX was observed in the nucleus of SK-BR-3 and MDA-MB-231. After 8 h, however, the DOX signal in the nucleus had increased by over five times in SK-BR-3 (results were statistically significant at  $p < 0.001$ ), while the

increase in MDA-MB-231 was not statistically significant. These results show that HER on the surface promoted the uptake specificity of DL-CNPs in HER2-positive breast cancer cells. The increased accumulation of DOX in the SK-BR-3 cells revealed that dual stimuli in cancer cells, low pH, and the high concentration of GSH facilitated the sequential and controlled release of DOX upon DL-CNP degradation. Similar to free DOX, the green fluorescence of the lysotracker indicated that the DOX released from the DL-CNPs was rapidly localized to the nucleus up to 8 h. DOX is known to inhibit cell proliferation by encoding the gene in the nucleus [57]. These results are consistent with the in vitro release profile in Figure 2b and cell viability results shown in Figure 3b above. These remarkable results confirm that DL-CNPs have great potential for use in the treatment of HER2-positive breast cancer.

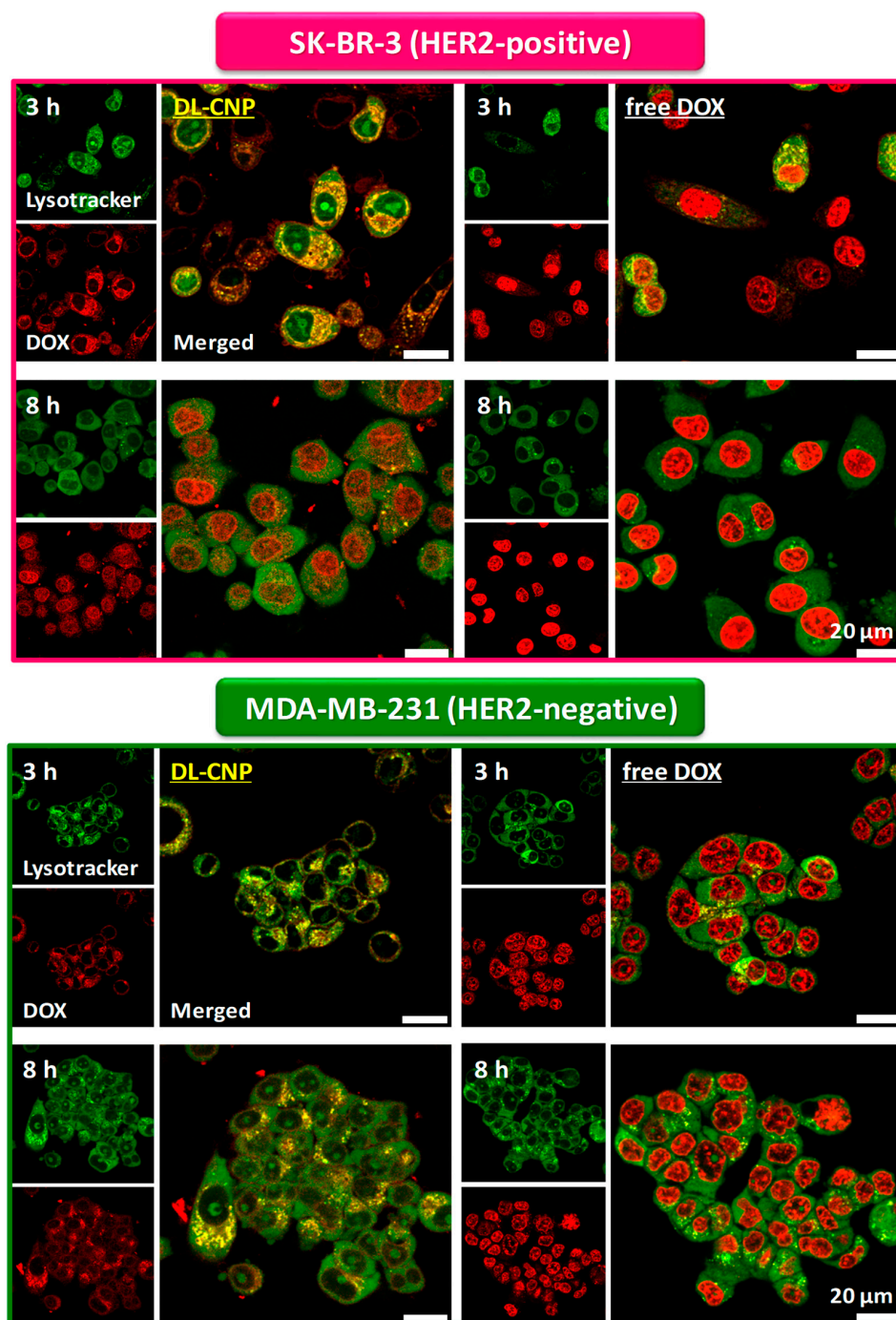


**Figure 4.** Confocal laser scanning microscopy (CLSM) images (scale bar = 20 μm) of SK-BR-3 and MDA-MB-231 cells incubated with DL-CNPs and free DOX for 3 and 8 h.

### 3.4. In Vivo Antitumor Efficacy and Toxicity of DL-CNPs

To evaluate the antitumor efficacy of the DL-CNPs against breast cancer, xenografts implanted with SK-BR-3 and MDA-MB-231 were treated with DL-CNPs, free DOX (an equivalent amount to the DOX in DL-CNPs), and PBS as the control. One mg DOX/kg body weight was weekly injected and the relative tumor growth over time was statistically analyzed by two-way analysis of variance (ANOVA) in GraphPad Prism 5 (GraphPad Software, La Jolla, CA, USA). As shown in Figure 5a, the SK-BR-3 tumor growth of the mice treated with DL-CNPs significantly decreased ( $p < 0.01$ ) compared with that of MDA-MB-231. Furthermore, immunohistochemical analysis using Ki-67 staining in Figure 5c supported that treatment of DL-CNPs exhibited more effective suppression of tumor proliferation than free DOX in the SK-BR-3 groups, which indicates a synergistically enhanced antitumor effect from the dual delivery of HER and DOX in DL-CNPs. However, the body weight was fairly constant, which was comparable to the control group during the treatment period (Figure 5b).

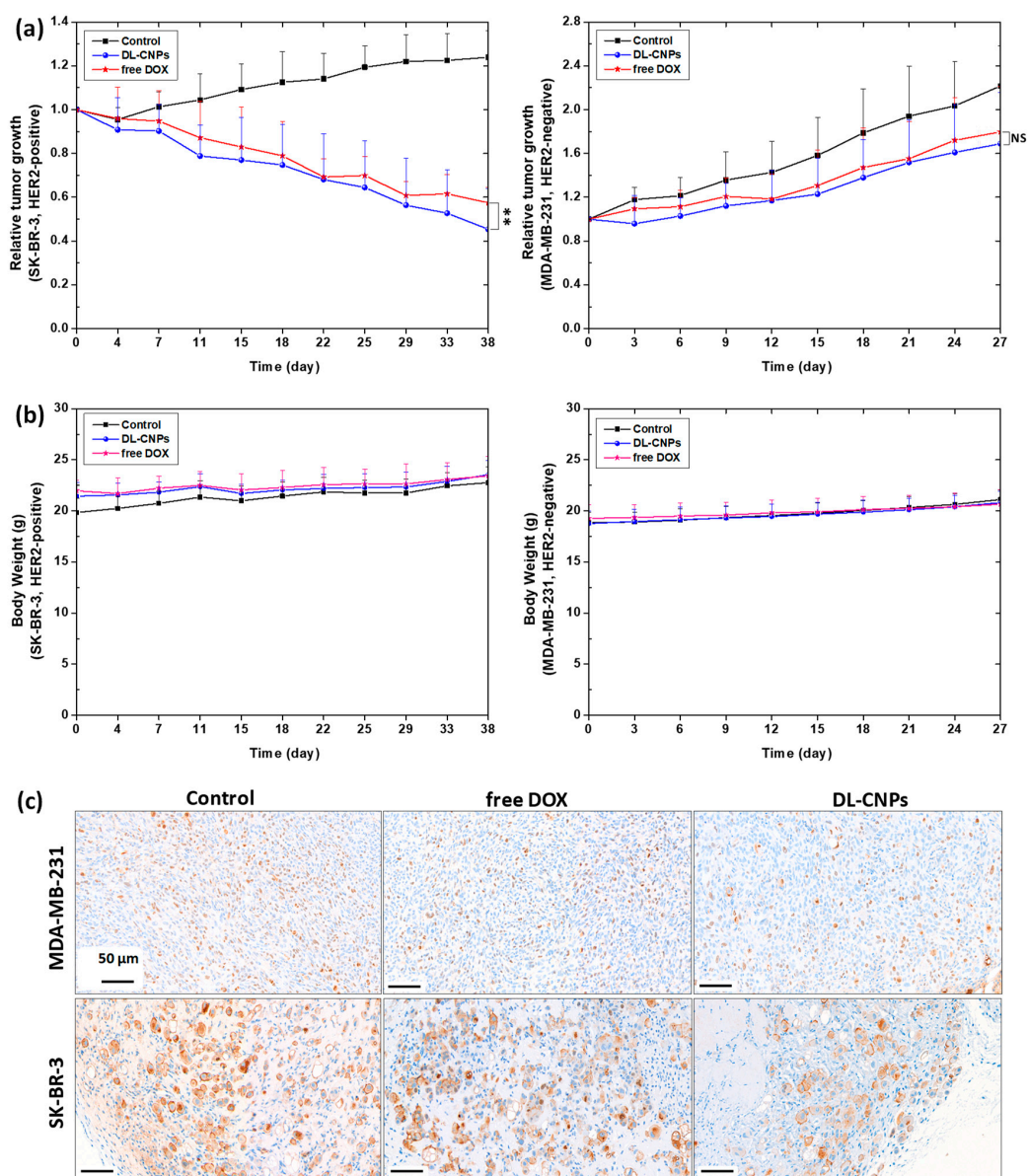


**Figure 5.** In vivo evaluation of DL-CNPs against HER2-positive and negative xenograft models based on (a) tumor growth, (b) body weight, and (c) histological analysis of Ki-67 expression in representative tumor tissue sections. For drug treatment groups, 1 mg/kg of DOX was injected weekly within 200  $\mu$ L saline ( $n \geq 7$  per group).

#### 4. Conclusions

Multi-functional CNPs engineered with PEG, HER, disulfides, and DOX were introduced as anticancer drug carriers for the treatment of HER2-positive cancer. HER on the surface of the nanoparticles promoted the cellular uptake of DS-CNPs into HER2-positive cells with low toxicity. DL-CNPs are stable under physiological conditions; however, DL-CNPs destabilized after endocytosis upon the cleavage of both disulfides, and acid-labile amide bonds enable the release of DOX in a controlled manner. Treatment with DL-CNPs resulted in the significant inhibition of tumor growth in xenografts derived from SK-BR-3 human breast cancer cells. Furthermore, the combined treatment of HER and DOX promoted an anticancer effect compared to the treatment with DOX alone. These remarkable results support that DL-CNP is an excellent platform for delivering HER2-positive breast cancer therapy.

**Supplementary Materials:** The following are available online at <http://www.mdpi.com/2079-4991/10/1/91/s1>, Figure S1. (a) Expression of HER2 in SK-BR-3 and MDA-BM-231 breast cancer cell lines.  $\beta$ -actin served as loading control; (b) Quantification of HER2 protein expression is given as intensity of  $\beta$ -actin-standardized HER2 levels in the cells.

**Author Contributions:** Conceptualization, N.R.K. and S.H.H.; Methodology, N.R.K., S.H.H., and J.S.L.; In vitro studies, S.Y.V. and J.S.L.; In vivo studies, S.-Y.K.; Validation, N.R.K., S.Y.V., and M.K.; Analysis, N.R.K., S.Y.V., and S.H.H.; Writing—original draft preparation, N.R.K., S.Y.V., and S.H.H.; Writing—review and editing, S.J.L.; Supervision, Y.-k.L., I.K.K., and S.J.O.; Project administration, N.R.K. All authors have read and agreed to the published version of the manuscript.

**Funding:** This research was supported by the Basic Science Research Program through the National Research Foundation of Korea (NRF) funded by the (NRF-2016R1A6A3A11934989 and NRF-2017R1D1A1B03034012); the Radiation Technology R&D program through the National Research Foundation of Korea funded by the Ministry of Science and ICT (NRF-2017M2A2A6A01070927); and the Korea Health Technology R&D Project through the Korea Health Industry Development Institute (KHIDI), funded by the Ministry of Health & Welfare, Republic of Korea (grant number: HI18C2383).

**Acknowledgments:** We thank the core facilities of the Confocal Microscope Core and the Optical Core at the ConveRgence mEDICine research center (CREDIT), Asan Medical Center for the use of their shared equipment, services and expertise. We also thank Md Nafiujjaman and Vishnu Revuri for providing carbon nanoparticles (CNPs).

**Conflicts of Interest:** The authors declare no conflicts of interest.

#### References

1. Wu, W.; Luo, L.; Wang, Y.; Wu, Q.; Dai, H.-B.; Li, J.-S.; Durkan, C.; Wang, N.; Wang, G.-X. Endogenous pH-responsive nanoparticles with programmable size changes for targeted tumor therapy and imaging applications. *Theranostics* **2018**, *8*, 3038–3058. [[CrossRef](#)]
2. Stubelius, A.; Sheng, W.; Lee, S.; Olejniczak, J.; Guma, M.; Almutairi, A. Disease-Triggered Drug Release Effectively Prevents Acute Inflammatory Flare-Ups, Achieving Reduced Dosing. *Small* **2018**, *14*. [[CrossRef](#)]
3. Li, L.; Yang, W.-W.; Xu, D.-G. Stimuli-responsive nanoscale drug delivery systems for cancer therapy. *J. Drug Target.* **2019**, *27*, 423–433. [[CrossRef](#)] [[PubMed](#)]
4. Travero, N.; Ricciarelli, R.; Nitti, M.; Marengo, B.; Furfaro, A.L.; Pronzato, M.A.; Marinari, U.M.; Domenicotti, C. Role of Glutathione in Cancer Progression and Chemoresistance. *J. Oxid. Med. Cell. Longev.* **2013**, *2013*, 10. [[CrossRef](#)]
5. Hassan, S.S.M.; Rechnitz, G.A. Determination of glutathione and glutathione reductase with a silver sulfide membrane electrode. *Anal. Chem.* **1982**, *54*, 1972–1976. [[CrossRef](#)]
6. Wen, H.; Dong, C.; Dong, H.; Shen, A.; Xia, W.; Cai, X.; Song, Y.; Li, X.; Li, Y.; Shi, D. Engineered redox-responsive PEG detachment mechanism in PEGylated nano-graphene oxide for intracellular drug delivery. *Small* **2012**, *8*, 760–769. [[CrossRef](#)]
7. Schafer, F.Q.; Buettner, G.R. Redox environment of the cell as viewed through the redox state of the glutathione disulfide/glutathione couple. *Free Radic. Biol. Med.* **2001**, *30*, 1191–1212. [[CrossRef](#)]
8. Raza, A.; Rasheed, T.; Nabeel, F.; Hayat, U.; Bilal, M.; Iqbal, H. Endogenous and exogenous stimuli-responsive drug delivery systems for programmed site-specific release. *Molecules* **2019**, *24*, 1117. [[CrossRef](#)]



9. Tsarevsky, N.V.; Matyjaszewski, K. Reversible Redox Cleavage/Coupling of Polystyrene with Disulfide or Thiol Groups Prepared by Atom Transfer Radical Polymerization. *Macromolecules* **2002**, *35*, 9009–9014. [[CrossRef](#)]
10. Li, C.; Madsen, J.; Armes, S.P.; Lewis, A.L. A new class of biochemically degradable, stimulus-responsive triblock copolymer gelators. *Angew. Chem. Int. Ed.* **2006**, *45*, 3510–3513. [[CrossRef](#)]
11. You, Y.-Z.; Zhou, Q.-H.; Manickam, D.S.; Wan, L.; Mao, G.-Z.; Oupicky, D. Dually Responsive Multiblock Copolymers via Reversible Addition-Fragmentation Chain Transfer Polymerization: Synthesis of Temperature- and Redox-Responsive Copolymers of Poly(N-isopropylacrylamide) and Poly(2-(dimethylamino)ethyl methacrylate). *Macromolecules* **2007**, *40*, 8617–8624. [[CrossRef](#)]
12. Talelli, M.; Rijcken, C.J.; Oliveira, S.; van der Meel, R.; van Bergen en Henegouwen, P.M.; Lammers, T.; van Nostrum, C.F.; Storm, G.; Hennink, W.E. Nanobody—Shell functionalized thermosensitive core-crosslinked polymeric micelles for active drug targeting. *J. Control. Release* **2011**, *151*, 183–192. [[CrossRef](#)]
13. Webb, B.A.; Chimenti, M.; Jacobson, M.P.; Barber, D.L. Dysregulated pH: A perfect storm for cancer progression. *Nat. Rev. Cancer* **2011**, *11*, 671–677. [[CrossRef](#)]
14. Mellman, I.; Fuchs, R.; Helenius, A. Acidification of the endocytic and exocytic pathways. *Annu. Rev. Biochem.* **1986**, *55*, 663–700. [[CrossRef](#)]
15. Thomas, M.; Ge, Q.; Lu, J.J.; Chen, J.; Klibanov, A. Cross-linked small polyethylenimines: While still nontoxic, deliver DNA efficiently to mammalian cells in vitro and in vivo. *Pharm. Res.* **2005**, *22*, 373–380. [[CrossRef](#)]
16. Russ, V.; Elfberg, H.; Thoma, C.; Kloeckner, J.; Ogris, M.; Wagner, E. Novel degradable oligoethylenimine acrylate ester-based pseudodendrimers for in vitro and in vivo gene transfer. *Gene Ther.* **2008**, *15*, 18. [[CrossRef](#)]
17. D'Souza, A.J.M.; Topp, E.M. Release from polymeric prodrugs: Linkages and their degradation. *J. Pharm. Sci.* **2004**, *93*, 1962–1979. [[CrossRef](#)]
18. Knorr, V.; Russ, V.; Allmendinger, L.; Ogris, M.; Wagner, E. Acetal Linked Oligoethylenimines for Use as pH-Sensitive Gene Carriers. *Bioconjug. Chem.* **2008**, *19*, 1625–1634. [[CrossRef](#)]
19. Wang, L.; Liu, G.; Wang, X.; Hu, J.; Zhang, G.; Liu, S. Acid-disintegratable polymersomes of pH-responsive amphiphilic diblock copolymers for intracellular drug delivery. *Macromolecules* **2015**, *48*, 7262–7272. [[CrossRef](#)]
20. Liu, B.; Thayumanavan, S. Substituent effects on the pH sensitivity of acetals and ketals and their correlation with encapsulation stability in polymeric nanogels. *J. Am. Chem. Soc.* **2017**, *139*, 2306–2317. [[CrossRef](#)]
21. Cha, C.; Shin, S.R.; Annabi, N.; Dokmeci, M.R.; Khademhosseini, A. Carbon-based nanomaterials: Multifunctional materials for biomedical engineering. *ACS Nano* **2013**, *7*, 2891–2897. [[CrossRef](#)]
22. Kumar, N.; Kumbhat, S. *Essentials in Nanoscience and Nanotechnology*; Wiley Online Library: Hoboken, NJ, USA, 2016.
23. Zhang, L.; Xia, J.; Zhao, Q.; Liu, L.; Zhang, Z. Functional Graphene Oxide as a Nanocarrier for Controlled Loading and Targeted Delivery of Mixed Anticancer Drugs. *Small* **2010**, *6*, 537–544. [[CrossRef](#)]
24. Sun, X.; Liu, Z.; Welsher, K.; Robinson, J.T.; Goodwin, A.; Zaric, S.; Dai, H. Nano-graphene oxide for cellular imaging and drug delivery. *Nano Res.* **2008**, *1*, 203–212. [[CrossRef](#)]
25. Ko, N.R.; Nafiujjaman, M.; Lee, J.S.; Lim, H.N.; Lee, Y.k.; Kwon, I.K. Graphene quantum dot-based theranostic agents for active targeting of breast cancer. *RSC Adv.* **2017**, *7*, 11420–11427. [[CrossRef](#)]
26. Ko, N.R.; Hong, S.H.; Nafiujjaman, M.; An, S.Y.; Revuri, V.; Lee, S.J.; Kwon, I.K.; Lee, Y.-K.; Oh, S.J. Glutathione-responsive PEGylated GQD-based nanomaterials for diagnosis and treatment of breast cancer. *J. Ind. Eng. Chem.* **2019**, *71*, 301–307. [[CrossRef](#)]
27. Ross, J.S.; Slodkowska, E.A.; Symmans, W.F.; Pusztai, L.; Ravdin, P.M.; Hortobagyi, G.N. The HER-2 receptor and breast cancer: Ten years of targeted anti-HER-2 therapy and personalized medicine. *Oncologist* **2009**, *14*, 320–368. [[CrossRef](#)]
28. Izumi, Y.; Xu, L.; di Tomaso, E.; Fukumura, D.; Jain, R.K. Tumour biology: Herceptin acts as an anti-angiogenic cocktail. *Nature* **2002**, *416*, 279–280. [[CrossRef](#)]
29. Bianchini, G.; Gianni, L. The immune system and response to HER2-targeted treatment in breast cancer. *Lancet Oncol.* **2014**, *15*, e58–e68. [[CrossRef](#)]



30. Tolaney, S.M.; Barry, W.T.; Dang, C.T.; Yardley, D.A.; Moy, B.; Marcom, P.K.; Albain, K.S.; Rugo, H.S.; Ellis, M.; Shapira, I.; et al. Adjuvant Paclitaxel and Trastuzumab for Node-Negative, HER2-Positive Breast Cancer. *N. Engl. J. Med.* **2015**, *372*, 134–141. [[CrossRef](#)]
31. Liu, X.; Liu, H.-J.; Cheng, F.; Chen, Y. Preparation and characterization of multi stimuli-responsive photoluminescent nanocomposites of graphene quantum dots with hyperbranched polyethylenimine derivatives. *Nanoscale* **2014**, *6*, 7453–7460. [[CrossRef](#)]
32. Stella, V.J.; Rao, V.M.; Zannou, E.A.; Zia, V. Mechanisms of drug release from cyclodextrin complexes. *Adv. Drug Deliv. Rev.* **1999**, *36*, 3–16. [[CrossRef](#)]
33. Saha, S.; Roy, A.; Roy, K.; Roy, M.N. Study to explore the mechanism to form inclusion complexes of  $\beta$ -cyclodextrin with vitamin molecules. *Sci. Rep.* **2016**, *6*, 35764. [[CrossRef](#)] [[PubMed](#)]
34. Wang, L.; Li, L.L.; Fan, Y.S.; Wang, H. Host–guest supramolecular nanosystems for cancer diagnostics and therapeutics. *Adv. Mater.* **2013**, *25*, 3888–3898. [[CrossRef](#)] [[PubMed](#)]
35. Vu, T.; Claret, F.X. Trastuzumab: Updated mechanisms of action and resistance in breast cancer. *Front. Oncol.* **2012**, *2*, 62. [[CrossRef](#)] [[PubMed](#)]
36. Thorn, C.F.; Oshiro, C.; Marsh, S.; Hernandez-Boussard, T.; McLeod, H.; Klein, T.E.; Altman, R.B. Doxorubicin pathways: Pharmacodynamics and adverse effects. *Pharm. Genom.* **2011**, *21*, 440–446. [[CrossRef](#)] [[PubMed](#)]
37. Borandeh, S.; Abdolmaleki, A.; Abolmaali, S.S.; Tamaddon, A.M. Synthesis, structural and in-vitro characterization of  $\beta$ -cyclodextrin grafted L-phenylalanine functionalized graphene oxide nanocomposite: A versatile nanocarrier for pH-sensitive doxorubicin delivery. *Carbohydr. Polym.* **2018**, *201*, 151–161. [[CrossRef](#)]
38. Pooresmaeil, M.; Namazi, H.  $\beta$ -Cyclodextrin grafted magnetic graphene oxide applicable as cancer drug delivery agent: Synthesis and characterization. *Mater. Chem. Phys.* **2018**, *218*, 62–69. [[CrossRef](#)]
39. Liang, W.; Huang, Y.; Lu, D.; Ma, X.; Gong, T.; Cui, X.; Yu, B.; Yang, C.; Dong, C.; Shuang, S.  $\beta$ -Cyclodextrin–Hyaluronic Acid Polymer Functionalized Magnetic Graphene Oxide Nanocomposites for Targeted Photo-Chemotherapy of Tumor Cells. *Polymers* **2019**, *11*, 133. [[CrossRef](#)]
40. Gao, N.; Xing, C.; Wang, H.; Feng, L.; Zeng, X.; Mei, L.; Peng, Z. pH-Responsive Dual Drug-Loaded Nanocarriers Based on Poly (2-Ethyl-2-Oxazoline) Modified Black Phosphorus Nanosheets for Cancer Chemo/Photothermal Therapy. *Front. Pharmacol.* **2019**, *10*. [[CrossRef](#)]
41. Swierczewska, M.; Lee, K.C.; Lee, S. What is the future of PEGylated therapies? *Expert Opin. Emerg.* **2015**, *20*, 531–536. [[CrossRef](#)]
42. Kurinamaru, T.; Shiraki, K. Noncovalent PEGylation of L-Asparaginase Using PEGylated Polyelectrolyte. *J. Pharm. Sci.* **2015**, *104*, 587–592. [[CrossRef](#)] [[PubMed](#)]
43. Reichert, C.; Borchard, G. Noncovalent PEGylation, an innovative subchapter in the field of protein modification. *J. Pharm. Sci.* **2016**, *105*, 386–390. [[CrossRef](#)] [[PubMed](#)]
44. Truffi, M.; Colombo, M.; Sorrentino, L.; Pandolfi, L.; Mazzucchelli, S.; Pappalardo, F.; Pacini, C.; Allevi, R.; Bonizzi, A.; Corsi, F. Multivalent exposure of trastuzumab on iron oxide nanoparticles improves antitumor potential and reduces resistance in HER2-positive breast cancer cells. *Sci. Rep.* **2018**, *8*, 6563. [[CrossRef](#)] [[PubMed](#)]
45. Dziawer, Ł.; Majkowska-Pilip, A.; Gawel, D.; Godlewska, M.; Pruszyński, M.; Jastrzębski, J.; Was, B.; Bilewicz, A. Trastuzumab-modified gold nanoparticles labeled with <sup>211</sup>At as a prospective tool for local treatment of HER2-positive breast cancer. *Nanomaterials* **2019**, *9*, 632. [[CrossRef](#)]
46. Tanaka, S.; Iwamoto, M.; Kimura, K.; Matsunami, N.; Morishima, H.; Yoshidome, K.; Nomura, T.; Morimoto, T.; Yamamoto, D.; Tsubota, Y. Phase II study of neoadjuvant anthracycline-based regimens combined with nanoparticle albumin-bound paclitaxel and trastuzumab for human epidermal growth factor receptor 2-positive operable breast cancer. *Clin. Breast Cancer* **2015**, *15*, 191–196. [[CrossRef](#)]
47. Yameen, B.; Choi, W.I.; Vilos, C.; Swami, A.; Shi, J.; Farokhzad, O.C. Insight into nanoparticle cellular uptake and intracellular targeting. *J. Control. Release* **2014**, *190*, 485–499. [[CrossRef](#)]
48. Vogel, C.L.; Cobleigh, M.A.; Tripathy, D.; Gutheil, J.C.; Harris, L.N.; Fehrenbacher, L.; Slamon, D.J.; Murphy, M.; Novotny, W.F.; Burchmore, M.; et al. First-Line Herceptin<sup>®</sup> Monotherapy in Metastatic Breast Cancer. *Oncology* **2001**, *61*, 37–42. [[CrossRef](#)]
49. Osoba, D.; Slamon, D.J.; Burchmore, M.; Murphy, M. Effects on Quality of Life of Combined Trastuzumab and Chemotherapy in Women With Metastatic Breast Cancer. *J. Clin. Oncol.* **2002**, *20*, 3106–3113. [[CrossRef](#)]
50. Montemurro, F.; Valabrega, G.; Aglietta, M. Trastuzumab-based combination therapy for breast cancer. *Expert Opin. Pharmacother.* **2004**, *5*, 81–96. [[CrossRef](#)]

51. Rodallec, A.; Brunel, J.-M.; Giacometti, S.; Maccario, H.; Correard, F.; Mas, E.; Orneto, C.; Savina, A.; Bouquet, F.; Lacarelle, B. Docetaxel–trastuzumab stealth immunoliposome: Development and in vitro proof of concept studies in breast cancer. *Int. J. Nanomed.* **2018**, *13*, 3451. [[CrossRef](#)]
52. Li, H.; Shao, B.; Yan, Y.; Song, G.; Liu, X.; Wang, J.; Liang, X. Efficacy and safety of trastuzumab combined with chemotherapy for first-line treatment and beyond progression of HER2-overexpressing advanced breast cancer. *Chin. J. Cancer Res.* **2016**, *28*, 330–338. [[CrossRef](#)] [[PubMed](#)]
53. Baselga, J. Herceptin® Alone or in Combination with Chemotherapy in the Treatment of HER2-Positive Metastatic Breast Cancer: Pivotal Trials. *Oncology* **2001**, *61*, 14–21. [[CrossRef](#)] [[PubMed](#)]
54. Cameron, D.; Piccart-Gebhart, M.J.; Gelber, R.D.; Procter, M.; Goldhirsch, A.; de Azambuja, E.; Castro, G.; Untch, M.; Smith, I.; Gianni, L.; et al. 11 years' follow-up of trastuzumab after adjuvant chemotherapy in HER2-positive early breast cancer: Final analysis of the HERceptin Adjuvant (HERA) trial. *Lancet* **2017**, *389*, 1195–1205. [[CrossRef](#)]
55. Singh, S.K.; Singh, S.; Lillard, J.W., Jr.; Singh, R. Drug delivery approaches for breast cancer. *Int. J. Nanomed.* **2017**, *12*, 6205–6218. [[CrossRef](#)]
56. Marty, M.; Cognetti, F.; Maraninchi, D.; Snyder, R.; Mauriac, L.; Tubiana-Hulin, M.; Chan, S.; Grimes, D.; Antón, A.; Lluch, A.; et al. Randomized Phase II Trial of the Efficacy and Safety of Trastuzumab Combined With Docetaxel in Patients With Human Epidermal Growth Factor Receptor 2–Positive Metastatic Breast Cancer Administered As First-Line Treatment: The M77001 Study Group. *J. Clin. Oncol.* **2005**, *23*, 4265–4274. [[CrossRef](#)]
57. Denard, B.; Seemann, J.; Chen, Q.; Gay, A.; Huang, H.; Chen, Y.; Ye, J. The Membrane-Bound Transcription Factor CREB3L1 Is Activated in Response to Virus Infection to Inhibit Proliferation of Virus-Infected Cells. *Cell Host Microbe* **2011**, *10*, 65–74. [[CrossRef](#)]



© 2020 by the authors. Licensee MDPI, Basel, Switzerland. This article is an open access article distributed under the terms and conditions of the Creative Commons Attribution (CC BY) license (<http://creativecommons.org/licenses/by/4.0/>).